AIAA JOURNAL
Vol. 30, No. 11, November 1992

Far-Field Computational Boundary Conditions for Two-Dimensional External Flow Problems

A. Verhoff,* D. Stookesberry,† and S. Agrawal‡
McDonnell Aircraft Company, St. Louis, Missouri 63166

Far-field computational boundary conditions for external flow problems have been developed from analytic solutions of the linearized steady-state Euler equations. These boundary conditions have improved accuracy compared with commonly used characteristic boundary conditions. The Euler equations are linearized about a constant pressure, rectilinear flow condition that truly represents conditions at infinity. Because the Euler equations are used to develop the boundary conditions, the flow crossing the boundary can be rotational. The boundary conditions can be used with any numerical Euler solution method and allow computational boundaries to be located very close to the nonlinear region of interest. This leads to a significant reduction in the number of grid points required for numerical solution. Numerical results are presented that show that the boundary conditions and far-field analytic solutions provide a smooth transition across a computational boundary to the true far-field conditions at infinity. They also demonstrate the synergism that can be realized from coupling analytic and computational methods. Computational efficiency gains are shown to be substantial.

Introduction

NUMERICAL solution procedures for nonlinear fluid dynamic equations usually use one or more artificial computational boundaries located at some distance from the primary region of interest to limit the physical domain to finite size. If the flow crossing such a boundary (either inflow or outflow) is subsonic, then some type of computational boundary conditions must be imposed that simulate the influence of the true far-field conditions at infinity. These boundary conditions must be such that waves crossing the boundary do not produce erroneous reflections back into the computational field to degrade the calculations. It is generally acknowledged that simply imposing conditions at infinity (such as the free-stream Mach number) at computational boundaries is usually inappropriate because they produce spurious reflections back into the computational domain. Standard practice has consisted of locating the boundaries quite far from the region of interest in an attempt to simplify the boundary condition models and minimize any effects of inconsistent modeling. The net effect is a significant increase in the number of grid points required for an accurate flowfield calculation.

A boundary modeling procedure for two-dimensional external flows is presented that alleviates the aforementioned difficulties and allows the computational boundaries to be located much closer to the nonlinear region of interest. The procedure is limited to steady, inviscid flow, although the flow can be rotational. It represents a logical first-order extension of the so-called characteristic (or zero-order) boundary conditions commonly used with inviscid numerical solution methods. It also illustrates a consistent method for coupling linearized analytic solutions with nonlinear numerical solutions by means of computational boundary conditions. The procedure is derived from a rigorous asymptotic expansion of the Euler equations. Therefore, it is applicable to flows that have strong entropy-producing effects (e.g., shock waves) within the computational region. Such effects can produce large variations in density and Mach number in the far field in the direction normal to streamlines (i.e., an entropy wake) that persist to infinity and that cannot be treated as small perturbations. A potential flow model (e.g., vortex correction due to lift) of such a far field containing rotational flow is inappropriate because the perturbations decay to zero at infinity.

A large number of boundary condition models have been proposed in the literature during the past two decades, and several of the more prominent works are cited herein.[1-5] The most noteworthy models are the nonreflecting boundary conditions that strive to suppress erroneous reflections from the boundary back into the computational domain. They are derived by linearizing the steady or unsteady fluid dynamic equations (usually Euler) about constant far-field conditions and solving the resulting system assuming a generalized waveform. However, their utility is compromised if strong rotational effects are produced in the computational domain because flow variables other than pressure and flow angle are not constant in the far field if the flow is treated as inviscid. In that case, linearization in terms of primitive or conservative variables yields perturbation quantities that do not vanish at infinity. Moreover, linearization about average far-field conditions becomes questionable if rotational effects are strong. It was shown earlier[6] that conditions are achieved readily for internal flows where a shock wave produces far-field Mach numbers downstream that vary by a factor of two. Streamline-normal gradient variations can be even more pronounced, which cause strong interactions to persist in the far field. It was also shown previously that a linearization with decaying perturbations is possible, but the linear system has nonconstant coefficients.[6]

The present analysis extends the work presented in Ref. 6 to external flows. The analysis is based on the previously proposed Riemann variable formulation of the Euler equations.[7] This represents a natural starting point because the zero-order (or characteristic) boundary conditions mentioned earlier are expressed in terms of Riemann variables. The equations are linearized about a constant pressure, rectilinear flow condition, which truly represents conditions at infinity. These linearized equations are assumed applicable in the far-field region beyond a computational boundary.

The first-order linearized Euler equations are solved using integral transform techniques and an iterative procedure. Coupling of these analytic solutions with the nonlinear numerical solution is accomplished by the boundary conditions in an unambiguous manner. The analytic solutions provide a smooth transition across the computational boundary to the

Presented as Paper 91-0630 at the AIAA 29th Aerospace Sciences Meeting, Reno, NV, Jan. 7-10, 1991; received Jan. 21, 1991; revision received March 5, 1992; accepted for publication March 9, 1992.

*McDonnell Douglas Corporation Fellow. Associate Fellow AIAA.
†Lead Engineer, Aerodynamics. Member AIAA.
‡Technical Specialist, Aerodynamics. Associate Fellow AIAA.

true far-field conditions at infinity. The first-order boundary conditions are in the form of distributions of flow quantities to be imposed along the boundary, not constant conditions. They represent a logical asymptotic extension of the zero-order conditions for external flows. The additional computational effort required to impose the first-order boundary conditions is modest. Furthermore, the boundary analysis can be coupled with any inviscid numerical solution method. It can also be coupled with a viscous method by expressing a wake as a vorticity distribution and convecting this distribution downstream via the Euler analytic model.[8]

Numerical results are presented for both inviscid isentropic and nonisentropic transonic airfoil flows. Two numerical analysis codes having different algorithmic formulations are used to demonstrate the versatility and consistency of the boundary condition procedure. Results obtained using the first-order boundary conditions are compared with those using zero-order conditions. It is found that the far-field boundaries can be located very close to the airfoil with negligible loss in accuracy. The reduction in number of grid points required (and computational cost) is shown to be substantial. The procedure can be extended to three dimensions with comparable reduction in grid sizes.

Perturbation Equations

The system of two-dimensional, steady, linearized Euler equations that describe first-order perturbations from a constant pressure state is derived from the Riemann variable formulation of Ref. 7. This formulation is used because of its close relationship with zero-order (or characteristic) boundary conditions commonly used in numerical solution of the nonlinear Euler equations. These equations are

$$\frac{\partial Q}{\partial t} + (q + a)\frac{\partial Q}{\partial s} = -\frac{\gamma - 1}{2} qaS \frac{\partial \theta}{\partial n} - \frac{\gamma - 1}{2} a\left(S - \frac{2}{\gamma - 1}\right)\left[\frac{\partial}{\partial s}\left(q - \frac{2}{\gamma - 1} a\right)\right] \tag{1}$$

$$\frac{\partial R}{\partial t} + (q - a)\frac{\partial R}{\partial s} = +\frac{\gamma - 1}{2} qaS \frac{\partial \theta}{\partial n} + \frac{\gamma - 1}{2} a\left(S - \frac{2}{\gamma - 1}\right)\left[\frac{\partial}{\partial s}\left(q + \frac{2}{\gamma - 1} a\right)\right] \tag{2}$$

$$\frac{\partial \theta}{\partial t} + q\frac{\partial \theta}{\partial s} = -\frac{a^2}{\gamma q}\frac{\partial P}{\partial n} \tag{3}$$

$$\frac{\partial S}{\partial t} + q\frac{\partial S}{\partial s} = 0 \tag{4}$$

Magnitude of velocity and speed of sound are denoted by q and a, respectively, and P is the logarithm of pressure. The Riemann-like variables Q and R are defined as $Q \equiv q + aS$ and $R \equiv q - aS$. The modified entropy is related to pressure p and density ρ according to

$$S \equiv \frac{1}{\gamma(\gamma - 1)}\left[2\gamma - \ell n\left(\frac{p}{\rho^\gamma}\right)\right] \qquad p \equiv \left(\frac{Q - R}{2S}\right)^{\frac{2\gamma}{\gamma - 1}} e^{\gamma\left(S - \frac{2}{\gamma - 1}\right)} \tag{5}$$

The flow angle is θ, time is denoted by t, and local distances along and normal to the streamline direction are denoted by s and n, respectively. The ratio of specific heats is γ.

For steady flow, the analysis can be greatly simplified by defining a new dependent variable $T \equiv Q - R$ and replacing Eqs. (1-4) by

$$(M^2 - 1)\frac{\partial T}{\partial s} + (\gamma - 1)\, qMS \frac{\partial \theta}{\partial n} = 0 \tag{6}$$

$$M^2 \frac{\partial \theta}{\partial s} + \frac{2}{\gamma - 1}\frac{1}{T}\frac{\partial T}{\partial n} + \frac{1}{S}\left(S - \frac{2}{\gamma - 1}\right)\frac{\partial S}{\partial n} = 0 \tag{7}$$

$$\frac{\partial S}{\partial s} = 0 \tag{8}$$

$$a^2 + \frac{\gamma - 1}{2} q^2 = 1 \tag{9}$$

The local Mach number is denoted by M. Equation (6) is obtained by subtracting Eqs. (1) and (2). Equation (9) is obtained by adding Eqs. (1) and (2) and integrating. The constant of integration, which is proportional to stagnation temperature, can be set to unity by proper choice of nondimensionalizing quantities.

According to Eq. (8), entropy remains constant along streamlines. In far-field regions of a flowfield where asymptotic conditions prevail, the flow can be treated as a perturbation to a constant pressure, rectilinear flow. Such regions occur near and beyond far-field computational boundaries. The dependent variables in Eqs. (6-8) can then be expanded in asymptotic series:

$$\begin{aligned} T &= T_\infty + T_1 + T_2 + \cdots \\ \theta &= \theta_\infty + \theta_1 + \theta_2 + \cdots \\ S &= S_\infty + S_1 + S_2 + \cdots \end{aligned} \tag{10}$$

The flow direction at infinity is assumed constant and denoted by θ_∞; the perturbation quantities T_i, θ_i, and S_i vanish at infinity. Entropy variation is not excluded so that the flow can be rotational in which case S_∞ and T_∞ are not constant, but vary normal to the streamline direction across the entropy wake. Furthermore, far-field entropy variations can be strong (i.e., not small perturbations). Note that T_∞ depends only on S_∞ (because p_∞ is constant).

Consistent with the expansions (10), spatial derivatives in Eqs. (6-8) can be approximated by

$$\begin{aligned} \frac{\partial}{\partial s} &= \cos\theta_\infty(1 - \tau\theta_1)\frac{\partial}{\partial x} + \cos\theta_\infty(\tau + \theta_1)\frac{\partial}{\partial y} + \cdots \\ \frac{\partial}{\partial n} &= -\cos\theta_\infty(\tau + \theta_1)\frac{\partial}{\partial x} + \cos\theta_\infty(1 - \tau\theta_1)\frac{\partial}{\partial y} + \cdots \end{aligned} \tag{11}$$

where x and y are reference Cartesian coordinates, θ is measured from the x axis, and $\tau \equiv \tan\theta_\infty$.

If expansions (10) and (11) are introduced into Eqs. (6-8), the resulting first-order perturbed Euler equations are

$$(M_\infty^2 - 1)\left[\frac{\partial T_1}{\partial x} + \tau\frac{\partial T_1}{\partial y} - \theta_1\left(\tau\frac{\partial T_\infty}{\partial x} - \frac{\partial T_\infty}{\partial y}\right)\right] + (\gamma - 1)q_\infty M_\infty S_\infty\left(\frac{\partial \theta_1}{\partial y} - \tau\frac{\partial \theta_1}{\partial x}\right) = 0 \tag{12}$$

$$\frac{\gamma - 1}{2} M_\infty^2 S_\infty\left(\frac{\partial \theta_1}{\partial x} + \tau\frac{\partial \theta_1}{\partial y}\right) + \frac{1}{2a_\infty}\left[\frac{\partial T_1}{\partial y} - \tau\frac{\partial T_1}{\partial x} - \frac{T_1}{T_\infty}\left(\frac{\partial T_\infty}{\partial y} - \tau\frac{\partial T_\infty}{\partial x}\right)\right] + \frac{S_1}{S_\infty}\left(\frac{\partial S_\infty}{\partial y} - \tau\frac{\partial S_\infty}{\partial x}\right) + \frac{\gamma - 1}{2}\left(S_\infty - \frac{2}{\gamma - 1}\right)\left(\frac{\partial S_1}{\partial y} - \tau\frac{\partial S_1}{\partial x}\right) = 0 \tag{13}$$

$$\frac{\partial S_1}{\partial x} + \tau\frac{\partial S_1}{\partial y} + \theta_1\left(\frac{\partial S_\infty}{\partial y} - \tau\frac{\partial S_\infty}{\partial x}\right) = 0 \tag{14}$$

Velocity, speed of sound, and Mach number at infinity are denoted by q_∞, a_∞, and M_∞, respectively, and may vary nor-

mal to the streamline direction downstream if the flow is nonisentropic. The fact that all dependent quantities are convected unchanged along rectilinear streamlines at infinity has been incorporated into the preceding equations.

Asymptotic expansions of the variables Q and R can also be defined as

$$Q = Q_\infty + Q_1 + Q_2 + \cdots \qquad R = R_\infty + R_1 + R_2 + \cdots \tag{15}$$

Using the definition of $T \equiv Q - R$ and the expansion (10), it follows that

$$T_\infty = Q_\infty - R_\infty \qquad T_1 = Q_1 - R_1 \qquad T_2 = Q_2 - R_2 \tag{16}$$

Introducing the expansions (10) and (15) into the algebraic equation (9) gives the first-order relationship

$$M_\infty(Q_1 - R_1) + \frac{\gamma - 1}{2} S_\infty M_\infty^2 (Q_1 + R_1) - 2q_\infty S_1 = 0 \tag{17}$$

This will be used later when the boundary conditions are derived.

Solution of Equations

Solutions of the first-order Eqs. (12–14) can be developed for various computational far-field boundary shapes. Shapes representative of C-grid topologies that are commonly used for numerical Euler solutions for airfoil flows have been chosen for this analysis. The first-order boundary conditions can then be developed from these analytic solutions.

When a C-grid topology is used for Euler calculations, the C portion of the outer boundary is selected such that inflow conditions exist along this portion and outflow conditions exist along the vertically oriented portion. A parabolic shape provides a simple analytic definition of the C portion of the boundary whereas the vertically oriented portion can easily be made linear. Modern grid generation methods, especially unstructured grid methods, can easily accommodate these outer boundary shapes.

Infinite Linear Boundary

The downstream boundary of a C grid can be made linear but has a finite length. Outflow conditions prevail along this boundary. If there is entropy produced within the computational domain, it crosses this downstream boundary and is convected into the far field. The downstream far-field region can be modeled by solving Eqs. (12–14) within a semi-infinite half-plane.

The perturbation equations are linear partial differential equations with nonconstant coefficients for nonisentropic flow because q_∞ and a_∞ vary in the downstream far field. The coefficients are constant if the flow is isentropic. Solution of the isentropic equations will be given first to illustrate the solution procedure. Solution of an approximate form of the nonisentropic equations will then be presented. For these developments, the boundary is assumed located at $x_d = 0$ (see Fig. 1); this choice is completely arbitrary.

Isentropic Flow

The isentropic form of the perturbation equations, Eqs. (12–14), is

$$\beta^2\left(\frac{\partial T_1}{\partial x} + \tau\frac{\partial T_1}{\partial y}\right) - 2q_\infty M_\infty\left(\frac{\partial \theta_1}{\partial y} - \tau\frac{\partial \theta_1}{\partial x}\right) = 0 \tag{18}$$

$$2q_\infty M_\infty\left(\frac{\partial \theta_1}{\partial x} + \tau\frac{\partial \theta_1}{\partial y}\right) + \frac{\partial T_1}{\partial y} - \tau\frac{\partial T_1}{\partial x} = 0 \tag{19}$$

For isentropic flow, the variables q_∞ and M_∞ are constant and $S_\infty = 2/(\gamma - 1)$. The parameter β is defined as $\sqrt{1 - M_\infty^2}$. Using Fourier transforms as outlined previously,[9] the solution of Eqs. (18) and (19) is

$$T_1 = \frac{2q_\infty M_\infty}{\beta\pi}\int_{-\infty}^{\infty} \frac{(y - t + \mu x)\theta_b(t)}{(y - t + \mu x)^2 + \nu^2 x^2}\,dt \tag{20}$$

$$\theta_1 = \frac{1}{\pi}\int_{-\infty}^{\infty} \frac{\nu x \theta_b(t)}{(y - t + \mu x)^2 + \nu^2 x^2}\,dt \tag{21}$$

where $\mu \equiv \tau M_\infty^2/(\beta^2 + \tau^2)$ and $\nu \equiv \beta(1 + \tau^2)/(\beta^2 + \tau^2)$. The boundary is assumed located at $x = 0$. The flow angle perturbation at the boundary is denoted by $\theta_b \equiv (\theta - \theta_\infty)|_{x=0}$. This distribution is provided by the nonlinear numerical solution.

Nonisentropic Flow

As shown previously,[6] Eqs. (12–14) are simplified by introducing a new variable σ defined by

$$S_\infty \equiv \frac{2}{\gamma - 1}(1 - \sigma) \tag{22}$$

where σ varies only in the direction normal to the streamlines across the entropy wake. Isentropic flow corresponds to $\sigma = 0$. Since σ is generally small, the thermodynamic relations can be approximated by

$$\begin{aligned} a_\infty &= \bar{a}_\infty(1 + \sigma) \qquad & q_\infty &= \bar{q}_\infty\left(1 - \frac{2}{\gamma - 1}\frac{\sigma}{\bar{M}_\infty^2}\right) \\ T_\infty &= \frac{4}{\gamma - 1}\bar{a}_\infty & M_\infty &= \bar{M}_\infty\left(1 - \frac{2}{\gamma - 1}\frac{\sigma}{\bar{q}_\infty^2}\right) \end{aligned} \tag{23}$$

Quadratic and higher-order terms in σ have been neglected. The reference quantities are defined as

$$\begin{aligned} \bar{a}_\infty &\equiv p_\infty^{(\gamma-1)/2\gamma} \\ \bar{q}_\infty &\equiv \sqrt{\frac{2}{\gamma - 1}(1 - \bar{a}_\infty^2)} \\ \bar{M}_\infty &\equiv \bar{q}_\infty/\bar{a}_\infty \end{aligned} \tag{24}$$

and are based on the assumption that the far-field pressure p_∞ is constant.

To illustrate the solution method for nonisentropic flow, Eqs. (12–14) can be further simplified by setting τ equal to zero, which orients the downstream boundary normal to the far-field flow direction. This is not overly restrictive since the

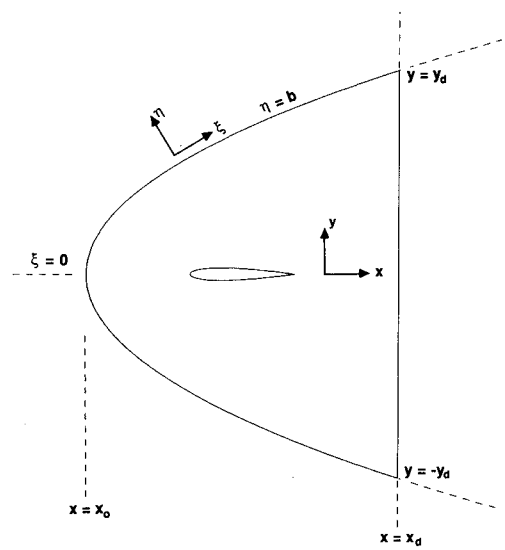

Fig. 1 Schematic of C-grid topology and boundary parameters.

body (e.g., airfoil) being analyzed can be arbitrarily oriented with respect to the boundary.

Introducing the approximations (23) into the governing Eqs. (12-14) and setting $\tau = 0$ gives

$$\left(\beta^2 + \frac{4}{\gamma - 1}\frac{\sigma}{\bar{a}_\infty^2}\right)\frac{\partial T_1}{\partial x} - 2\bar{q}_\infty \bar{M}_\infty \omega(\sigma)\frac{\partial \theta_1}{\partial y} = 0 \tag{25}$$

$$2\bar{q}_\infty \bar{M}_\infty \omega(\sigma)\frac{\partial \theta_1}{\partial x} + \frac{\partial T_1}{\partial y} = 2\bar{a}_\infty \frac{\partial}{\partial y}(\sigma S_1) \tag{26}$$

$$\frac{\partial S_1}{\partial x} - \frac{2}{\gamma - 1}\frac{d\sigma}{dy}\theta_1 = 0 \tag{27}$$

where $\beta \equiv \sqrt{1 - \bar{M}_\infty^2}$ and $\omega(\sigma) \equiv 1 - 4/(\gamma - 1)(\sigma/\bar{q}_\infty^2)$.

Equation (27) suggests that S_1 is of higher order than T_1 or θ_1. If so, then the right-hand side of Eq. (26) can be set to zero and Eq. (27) becomes decoupled. Validity of this assumption can be verified later by evaluating numerical results. The final system of equations is therefore

$$\left(\beta^2 + \frac{4}{\gamma - 1}\frac{\sigma}{\bar{a}_\infty^2}\right)\frac{\partial T_1}{\partial x} - 2\bar{q}_\infty \bar{M}_\infty \omega(\sigma)\frac{\partial \theta_1}{\partial y} = 0 \tag{28}$$

$$2\bar{q}_\infty \bar{M}_\infty \omega(\sigma)\frac{\partial \theta_1}{\partial x} + \frac{\partial T_1}{\partial y} = 0 \tag{29}$$

Using Fourier transforms as outlined previously,[9] the approximate solution for θ_1 is

$$\theta_1 = \frac{\beta}{\pi}\int_{-\infty}^{\infty}\left[1 + \frac{4}{\gamma - 1}\frac{\bar{M}_\infty^2}{\beta^2 \bar{q}_\infty^2}\sigma(t)\right]\theta_b(t)\frac{x}{\beta^2(y-t)^2 + x^2}\,dt$$
$$- \frac{2}{\gamma - 1}\frac{1}{\pi\beta^2\bar{q}_\infty^2}\int_{-\infty}^{\infty}\sigma'(t)\int_{-\infty}^{\infty}\theta_b'(u)\tan^{-1}\left(\frac{x}{z}\right)du\,dt$$
$$- \frac{4}{\gamma - 1}\frac{\bar{M}_\infty^2}{\pi\bar{q}_\infty^2}\int_{-\infty}^{\infty}\sigma(t)\int_{-\infty}^{\infty}\theta_b(u)\frac{zx}{(z^2 + x^2)^2}\,du\,dt \tag{30}$$

where $z \equiv \beta(|y - t| + |u - t|)$. For isentropic flow this solution reduces to the familiar Poisson integral formula (21).

The approximate solution for T_1 can be obtained by integrating Eq. (28) rewritten in the form

$$\frac{\beta^2}{2\bar{q}_\infty \bar{M}_\infty}\frac{\partial T_1}{\partial x} = \frac{\partial \theta_1}{\partial y} - \frac{4}{\gamma - 1}\frac{\beta\sigma}{\pi\bar{q}_\infty^2}\frac{\partial}{\partial x}\int_{-\infty}^{\infty}\theta_b(t)g\,dt \tag{31}$$

where $g \equiv (y - t)/[\beta^2(y - t)^2 + x^2]$. The solution (20) with $\tau = 0$ has been used to approximate those terms multiplied by σ. Carrying out the integration with respect to x gives

$$T_1 = \frac{2\bar{q}_\infty \bar{M}_\infty}{\beta\pi}\int_{-\infty}^{\infty}\theta_b(t)g\,dt + \frac{8}{\gamma - 1}\frac{\bar{M}_\infty}{\pi\beta\bar{q}_\infty}$$
$$\times\left[\bar{M}_\infty^2\int_{-\infty}^{\infty}\sigma(t)\theta_b(t)g\,dt - \sigma(y)\int_{-\infty}^{\infty}\theta_b(t)g\,dt\right]$$
$$+ \frac{2}{\gamma - 1}\frac{\bar{M}_\infty}{\pi\beta^3\bar{q}_\infty}\left[\int_{-\infty}^{y}\sigma'(t)\int_{-\infty}^{\infty}\theta_b'(u)\log(z^2 + x^2)\,du\,dt\right.$$
$$\left. - \int_{y}^{\infty}\sigma'(t)\int_{-\infty}^{\infty}\theta_b'(u)\log(z^2 + x^2)\,du\,dt\right]$$
$$+ \frac{4}{\gamma - 1}\frac{\bar{M}_\infty^3}{\pi\beta\bar{q}_\infty}\left\{\int_{-\infty}^{y}\sigma(t)\int_{-\infty}^{\infty}\theta_b(u)\left[\frac{1}{z^2 + x^2} - \frac{2z^2}{(z^2 + x^2)^2}\right]du\,dt\right.$$
$$\left. - \int_{y}^{\infty}\sigma(t)\int_{-\infty}^{\infty}\theta_b(u)\left[\frac{1}{z^2 + x^2} - \frac{2z^2}{(z^2 + x^2)^2}\right]du\,dt\right\} \tag{32}$$

Repeating this iterative process results in more accurate approximations to the solution of the system of Eqs. (28) and (29). Whether the additional effort is warranted can be decided by assessing the numerical accuracy of the solutions (30) and (32).

Although considerably more complex, the more general solution for nonzero τ can be obtained by following the same procedures used in obtaining the solutions (30) and (32).

Parabolic Boundary

The upstream boundary of a C-grid topology can be made parabolic in shape as shown in Fig. 1. This places no restrictions on modern grid generation procedures. The shape is chosen such that inflow conditions exist along the boundary. The onset flow crossing such a boundary for external flow problems is typically isentropic so that the perturbation equations, Eqs. (18) and (19), are applicable upstream of the boundary. Note that q_∞ and M_∞ are constant for isentropic flow.

Using complex variable notation, the parabolic transformation

$$x + iy = \zeta^2 + k \qquad \zeta \equiv \xi + i\eta \tag{33}$$

produces a (ξ, η) coordinate system that aligns with the parabolic boundary. The boundary shape as shown in Fig. 1 is defined by $y = y_d\sqrt{(x - x_0)/(x_d - x_0)}$. If the coordinate line $\eta = b$ is made to coincide with the boundary, then $b = y_d/(2\sqrt{x_d - x_0})$ and $k = x_0 + b^2$. Note that for analysis of this upstream boundary $x = y = 0$ corresponds to an arbitrary reference point within the computational domain (e.g., airfoil leading edge).

The scaling transformation defined by

$$\bar{x} \equiv \frac{x}{\beta} \qquad \bar{y} \equiv y \qquad \bar{b} \equiv \sqrt{\beta}b$$
$$\bar{T} \equiv \frac{T_1}{2q_\infty M_\infty} \qquad \bar{\theta} \equiv \frac{\theta_1}{\beta} \tag{34}$$

transforms Eqs. (18) and (19) into

$$\frac{\partial \bar{T}}{\partial \bar{x}} - \frac{\partial \bar{\theta}}{\partial \bar{y}} = -\tau\beta\left(\frac{\partial \bar{T}}{\partial \bar{y}} + \frac{1}{\beta^2}\frac{\partial \bar{\theta}}{\partial \bar{x}}\right) \tag{35}$$

$$\frac{\partial \bar{T}}{\partial \bar{y}} + \frac{\partial \bar{\theta}}{\partial \bar{x}} = -\tau\beta\left(\frac{\partial \bar{\theta}}{\partial \bar{y}} - \frac{1}{\beta^2}\frac{\partial \bar{T}}{\partial \bar{x}}\right) \tag{36}$$

Application of the parabolic transformation (33) to these equations gives

$$\frac{\partial T}{\partial \xi} - \frac{\partial \theta}{\partial \eta} = \frac{-\tau\beta}{\xi^2 + \eta^2}\left[\xi^2\left(\frac{\partial T}{\partial \eta} + \frac{1}{\beta^2}\frac{\partial \theta}{\partial \xi}\right)\right.$$
$$\left. + \eta^2\left(\frac{\partial \theta}{\partial \xi} + \frac{1}{\beta^2}\frac{\partial T}{\partial \eta}\right) - \frac{M_\infty^2}{\beta^2}\xi\eta\left(\frac{\partial T}{\partial \xi} + \frac{\partial \theta}{\partial \eta}\right)\right] \tag{37}$$

$$\frac{\partial T}{\partial \eta} + \frac{\partial \theta}{\partial \xi} = \frac{-\tau\beta}{\xi^2 + \eta^2}\left[\xi^2\left(\frac{\partial \theta}{\partial \eta} - \frac{1}{\beta^2}\frac{\partial T}{\partial \xi}\right)\right.$$
$$\left. - \eta^2\left(\frac{\partial T}{\partial \xi} - \frac{1}{\beta^2}\frac{\partial \theta}{\partial \eta}\right) + \frac{M_\infty^2}{\beta^2}\xi\eta\left(\frac{\partial T}{\partial \eta} - \frac{\partial \theta}{\partial \xi}\right)\right] \tag{38}$$

The overbars have been deleted to simplify notation.

Since τ is generally small, Eqs. (37) and (38) can be solved by iteration (as in the previous section). The first approximation (assuming $\tau = 0$) can be obtained directly from the solutions (20) and (21) as

$$\bar{T} = \frac{1}{\pi}\int_{-\infty}^{\infty}\frac{(\eta - \bar{b})T_b(t)}{(\xi - t)^2 + (\eta - \bar{b})^2}\,dt \tag{39}$$

$$\tilde{\theta} = \frac{1}{\pi} \int_{-\infty}^{\infty} \frac{(\xi - t) T_b(t)}{(\xi - t)^2 + (\eta - \bar{b})^2} \, dt \tag{40}$$

where T_b represents the distribution of the perturbation quantity $\bar{T}$ at the parabolic scaled boundary $\eta = \bar{b}$. Using these results in the right-hand sides of Eqs. (37) and (38) gives

$$\frac{\partial T}{\partial \xi} - \frac{\partial \theta}{\partial \eta} = \frac{\tau M_\infty^2}{\beta} \frac{1}{\xi^2 + \eta^2} \left[(\xi^2 - \eta^2) \frac{\partial \tilde{T}}{\partial \eta} + 2\xi\eta \frac{\partial \tilde{T}}{\partial \xi} \right] \equiv \frac{\partial U}{\partial \eta} \tag{41}$$

$$\frac{\partial T}{\partial \eta} + \frac{\partial \theta}{\partial \xi} = \frac{\tau M_\infty^2}{\beta} \frac{1}{\xi^2 + \eta^2} \left[(\xi^2 - \eta^2) \frac{\partial \tilde{T}}{\partial \xi} - 2\xi\eta \frac{\partial \tilde{T}}{\partial \eta} \right] \equiv \frac{\partial V}{\partial \xi} \tag{42}$$

The solution of the system (41) and (42) can be expressed as

$$T = \frac{\partial I}{\partial \xi}, \qquad \theta = V - \frac{\partial I}{\partial \eta} \tag{43}$$

where I satisfies

$$\frac{\partial^2 I}{\partial \xi^2} + \frac{\partial^2 I}{\partial \eta^2} = \frac{\partial}{\partial \eta} (U + V) \tag{44}$$

Carrying out the integrations for U and V, as defined by Eqs. (41) and (42), gives

$$U + V = \frac{-2\tau M_\infty^2}{\pi\beta} \operatorname{Im} \int_{-\infty}^{\infty} \left[\frac{\zeta}{t - i\bar{b}} \frac{1}{t - i\bar{b} - \bar{\zeta}} + \frac{\zeta}{(t - i\bar{b})^2} \log\left(\frac{\bar{\zeta}}{t - i\bar{b} - \bar{\zeta}} \right) \right] T_b(t) \, dt \tag{45}$$

and

$$V = \frac{-\tau M_\infty^2}{\pi\beta} \operatorname{Im} \int_{-\infty}^{\infty} \left[\frac{2i\eta + t - i\bar{b}}{t - i\bar{b}} \frac{1}{t - i\bar{b} - \bar{\zeta}} + \frac{2i\eta}{(t - i\bar{b})^2} \log\left(\frac{\bar{\zeta}}{t - i\bar{b} - \bar{\zeta}} \right) \right] T_b(t) \, dt \tag{46}$$

where the complex conjugate $\bar{\zeta} = \xi - i\eta$. The result, Eq. (45), can be used to obtain a particular solution of Eq. (44) by integral transforms, which gives

$$I = \frac{-\tau M_\infty^2}{\pi\beta} \operatorname{Im} \int_{-\infty}^{\infty} \left[\frac{\xi\eta}{t - i\bar{b} - \bar{\zeta}} + \frac{i\eta^2}{t - i\bar{b}} \log\left(\frac{\bar{\zeta}}{t - i\bar{b} - \bar{\zeta}} \right) \right] \frac{T_b(t)}{t - i\bar{b}} \, dt \tag{47}$$

It is easily verified that this result is a particular solution of Eq. (44).

For use in Eq. (43), derivatives of the solution I are

$$\frac{\partial I}{\partial \xi} = \frac{-\tau M_\infty^2}{\pi\beta} \operatorname{Im} \int_{-\infty}^{\infty} \left[\frac{\eta}{t - i\bar{b} - \bar{\zeta}} + \frac{\xi\eta}{(t - i\bar{b} - \bar{\zeta})^2} + \frac{i\eta^2}{\bar{\zeta}} \frac{1}{t - i\bar{b} - \bar{\zeta}} \right] \frac{T_b(t)}{t - i\bar{b}} \, dt \tag{48}$$

and

$$\frac{\partial I}{\partial \eta} = \frac{-\tau M_\infty^2}{\pi\beta} \operatorname{Im} \int_{-\infty}^{\infty} \left[\frac{\xi}{t - i\bar{b} - \bar{\zeta}} - \frac{i\xi\eta}{(t - i\bar{b} - \bar{\zeta})^2} + \frac{\eta^2}{\bar{\zeta}} \frac{1}{t - i\bar{b} - \bar{\zeta}} + \frac{2i\eta}{t - i\bar{b}} \log\left(\frac{\bar{\zeta}}{t - i\bar{b} - \bar{\zeta}} \right) \right] \frac{T_b(t)}{t - i\bar{b}} \, dt \tag{49}$$

Denoting contributions of the particular solution (47) by T_I and θ_I, then

$$T_I = \frac{-\tau M_\infty^2}{\pi\beta} \operatorname{Im} \int_{-\infty}^{\infty} \left[\frac{\eta}{t - i\bar{b} - \bar{\zeta}} + \frac{\xi\eta}{(t - i\bar{b} - \bar{\zeta})^2} + \frac{i\eta^2}{\bar{\zeta}} \frac{1}{t - i\bar{b} - \bar{\zeta}} \right] \frac{T_b(t)}{t - i\bar{b}} \, dt \tag{50}$$

$$\theta_I = \frac{-\tau M_\infty^2}{\pi\beta} \operatorname{Re} \left[\frac{\xi\eta}{\bar{\zeta}^2} \int_{-\infty}^{\infty} \left(\frac{1}{t - i\bar{b} - \bar{\zeta}} - \frac{1}{t - i\bar{b}} \right) T_b(t) \, dt \right] \tag{51}$$

The solution component θ_I is obtained by combining Eqs. (46) and (49).

The analysis is further simplified by introducing constants B_1 and B_2 and a boundary function w defined as

$$B_1 \equiv \int_{-\infty}^{\infty} \frac{t^2 - \bar{b}^2}{(t^2 + \bar{b}^2)^2} T_b(t) \, dt \tag{52}$$

$$B_2 \equiv \int_{-\infty}^{\infty} \frac{t}{(t^2 + \bar{b}^2)^2} T_b(t) \, dt \tag{53}$$

$$w(\xi) \equiv \lim_{\eta \to \bar{b}} \int_{-\infty}^{\infty} \frac{T_b'(t)}{t^2 + \bar{b}^2} \frac{\xi - t}{(\xi - t)^2 + (\eta - \bar{b})^2} \, dt \tag{54}$$

Using these quantities, the boundary distribution produced by the solution component T_I can be expressed as

$$B(\xi) = \frac{\tau M_\infty^2}{\pi\beta} \left[\frac{\pi\bar{b}\xi^2}{\xi^2 + \bar{b}^2} T_b'(\xi) + \bar{b}^2 \xi w(\xi) - \frac{\bar{b}^2 \xi}{\xi^2 + \bar{b}^2} (B_1 + 2\xi B_2) \right] \tag{55}$$

To satisfy the correct conditions at the boundary with respect to information propagating upstream to the boundary from the numerical solution, this distribution induced by the particular solution T_I must be negated by including a solution of the homogeneous portion of Eqs. (35) and (36). The second approximation to the solution of Eqs. (35) and (36) can then be expressed as

$$T = \frac{1}{\pi} \int_{-\infty}^{\infty} \frac{\eta - \bar{b}}{(\xi - t)^2 + (\eta - \bar{b})^2} [T_b(t) - B(t)] \, dt + T_I \tag{56}$$

$$\theta = \frac{1}{\pi} \int_{-\infty}^{\infty} \frac{\xi - t}{(\xi - t)^2 + (\eta - \bar{b})^2} [T_b(t) - B(t)] \, dt + \theta_I \tag{57}$$

The transformations (33) and (34) relate these solutions back to the physical plane.

Repeating the iterative process [i.e., substituting the second approximation into the right-hand sides of Eqs. (41) and (42) and solving] would produce a more accurate third approximation, but the additional effort is probably not warranted. This can be verified by assessing the numerical results.

Development of Boundary Conditions

Examination of Eqs. (1-4) shows that at a subsonic far-field computational boundary there are three downstream-propagating waves and one upstream-propagating wave. Therefore, the information available from the numerical solution is not complete and differs at upstream and downstream boundaries. The missing information must be provided by the boundary conditions. If the flow is supersonic, all waves are downstream propagating and specification of boundary conditions is straightforward.

Far-field computational boundary conditions (subsonic) can be developed from the linearized Euler solutions obtained earlier. These solutions are assumed valid in the region beyond the computational boundaries where asymptotic conditions exist. Within the computational boundaries, the full nonlinear Euler equations must be solved numerically. The boundary conditions provide for a smooth coupling of the nonlinear and

linear solutions so that the true conditions at infinity can be imposed.

Outflow Boundary Conditions

Analytic solutions of the linearized Euler equations that describe the far-field flow beyond an infinite linear boundary were obtained for both isentropic and nonisentropic conditions. These solutions can be used to model the flowfield beyond the downstream computational boundary of a C-grid topology.

Isentropic Flow

For isentropic conditions there are two waves propagating information to the downstream (outflow) boundary from the numerical solution and one wave propagating information upstream from outside the computational domain. The numerical solution provides boundary distributions of flow angle θ and the Riemann variable $Q \equiv q + aS$. Note that $S = 2/(\gamma - 1)$ for isentropic flow. The information required from outside the computational domain is provided by the solution (20).

Using the definition of $T \equiv Q - R$, the expansions (10), and the solution (20), the boundary distribution of the Riemann variable $R \equiv q - aS$ (i.e., the boundary conditions, $R_{bc} = R_\infty + R_1$) is calculated according to

$$R_{bc} = Q_{\text{num}} - \frac{4}{\gamma - 1} a_\infty - \frac{2q_\infty M_\infty}{\beta\pi} \lim_{x \to 0} \int_{-\infty}^{\infty} \frac{(y - t + \mu x)\theta_b(t)}{(y - t + \mu x)^2 + \nu^2 x^2} \, dt \tag{58}$$

The boundary distribution of Q propagated by the nonlinear numerical solution to the boundary is denoted by Q_{num}. The boundary is arbitrarily assumed located at $x = 0$. The integration can be carried out numerically using, for example, trapezoidal integration. The boundary distribution θ_b is obtained from the distribution of θ propagated to the boundary by the numerical solution.

The numerical solution provides a distribution of θ_b only to the outer corners of the C-grid boundary denoted by $y = \pm y_d$ in Fig. 1. The distribution can be extrapolated beyond the corners using a low-order polynomial in inverse powers of y, such as $\theta_b = C_1 |y|^{-1} + C_2 y^{-2}$. Beyond the corners, θ_b is relatively small and contributes very little to the integration required in Eq. (58).

Many numerical solution algorithms for the Euler equations use so-called characteristic far-field boundary conditions in which a constant R_∞ is imposed at an outflow boundary. The boundary condition (58) therefore represents a logical first-order asymptotic extension to the characteristic (or zero-order) boundary conditions.

Nonisentropic Flow

For nonisentropic conditions, an additional entropy wave crosses the downstream boundary from the numerical solution. If streamline curvature downstream of the boundary is neglected, then the secondary perturbation variable σ defined by Eq. (22) can be approximated from

$$\sigma(y) = 1 - \frac{\gamma - 1}{2} S_{\text{num}} \tag{59}$$

where S_{num} is the entropy distribution propagated to the boundary by the nonlinear numerical solution.

Using the approximate solution for T_1 given by Eq. (32), the distribution of the Riemann variable R on the boundary (i.e., the boundary conditions) is calculated according to

$$R_{bc} = Q_{\text{num}} - \frac{4}{\gamma - 1} \bar{a}_\infty - \lim_{x \to 0} (T_1) \tag{60}$$

The approximation (23) for T_∞ has been used, and Q_{num} again denotes the boundary distribution of Q obtained from the nonlinear numerical solution. This expression reduces to the boundary distribution (58) for isentropic flow.

Inflow Boundary Conditions

The linearized solutions (56) and (57) can be used to simulate the isentropic flowfield upstream of a parabolic C-grid topology. At an upstream isentropic inflow boundary, there are two waves propagating information to the boundary from outside the computational domain and one wave propagating information upstream from the numerical solution. The solution (57) provides one of the missing pieces of information from outside the computational domain; the remaining information is provided by the perturbation relation (17).

The perturbation relationship (17) applied at the computational boundary $\eta = \bar{b}$, assuming isentropic conditions [i.e., $S_\infty = 2/(\gamma - 1)$, $S_1 = 0$], yields the distribution of the Riemann variable $Q = Q_\infty + Q_1$ (i.e., the first of two boundary conditions) as

$$Q_{bc} = Q_\infty + \frac{1 - M_\infty}{1 + M_\infty} (R_{\text{num}} - R_\infty) \tag{61}$$

where $R_{\text{num}} - R_\infty = R_1$. The boundary distribution of R propagated by the nonlinear numerical solution to the boundary is denoted by R_{num}. Likewise, the boundary distribution of T_b needed in the solution (57) can be obtained from Eq. (17) and the transformation (34) as

$$T_b = -\frac{1}{q_\infty(1 + M_\infty)} (R_{\text{num}} - R_\infty) \tag{62}$$

The distribution of flow angle on the computational boundary (i.e., the remaining boundary condition, $\theta_{bc} = \theta_\infty + \theta_1$) is provided by the solution (57) as

$$\theta_{bc} = \theta_\infty + \frac{\beta}{\pi} \lim_{\eta \to \bar{b}} \int_{-\infty}^{\infty} \frac{\xi - t}{(\xi - t)^2 + (\eta - \bar{b})^2} [T_b(t) - B(t)] \, dt - \frac{\tau M_\infty^2}{\pi} \operatorname{Im} \left[\frac{i\xi\bar{b}}{\bar{\xi}^2} \lim_{\eta \to \bar{b}} \int_{-\infty}^{\infty} \left(\frac{1}{t - i\bar{b} - \bar{\xi}} - \frac{1}{t - i\bar{b}} \right) T_b(t) \, dt \right] \tag{63}$$

The function B is composed of boundary integrals and is defined by Eq. (55).

The transformations (33) and (34) relate ξ and η to the physical variables x and y according to

$$\frac{x}{\beta} + iy = (\xi + i\eta)^2 + \frac{x_0}{\beta} + \beta b^2 \tag{64}$$

Note that $x = y = 0$ corresponds to some arbitrary reference point within the computational domain and may differ from that chosen for the downstream boundary analysis. As in the case of θ_b at the downstream boundary, T_b must be extended along the parabolic portion of the boundary downstream of $x = x_d$ by some type of approximation compatible with the downstream far-field solution (see Fig. 1). Extrapolation using a low-order polynomial in inverse powers of ξ is sufficient.

Zero-order (or characteristic) boundary conditions would consist of imposing the constant values Q_∞ and θ_∞ at an upstream boundary. It is evident that both of the upstream boundary condition relations (61) and (63) represent logical first-order asymptotic extensions of the commonly used zero-order conditions.

Applications

The boundary condition procedures developed earlier herein have been successfully implemented in several two-dimensional Euler codes. Airfoil flowfields were calculated using

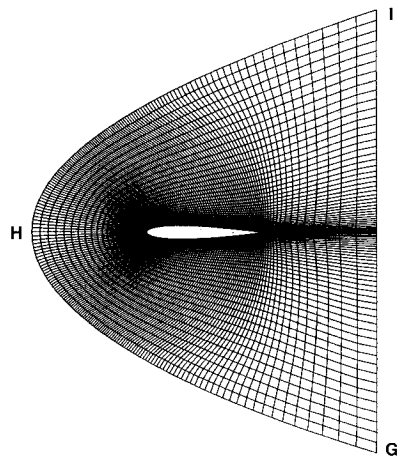

Fig. 2 Core grid ($\overline{GHIG}$) for NACA 0012 airfoil.

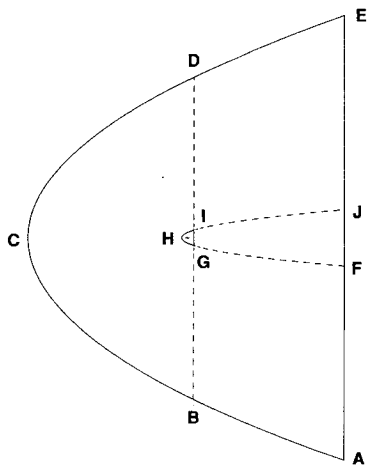

Fig. 3 Relative boundary locations of baseline ($\overline{ACEA}$) and core grids.

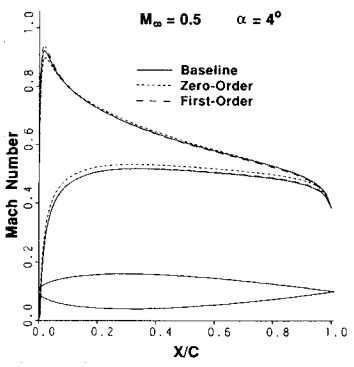

Fig. 4a ET12D surface Mach number predictions with outer boundary at $\overline{GHIG}$.

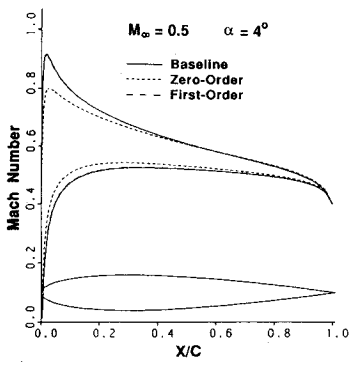

Fig. 4b FLO672D surface Mach number predictions with outer boundary at $\overline{GHIG}$.

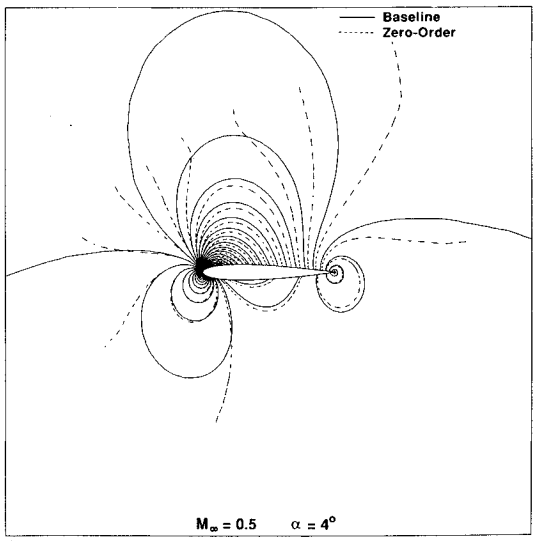

Fig. 5a Pressure contours predicted by ET12D using zero-order boundary conditions.

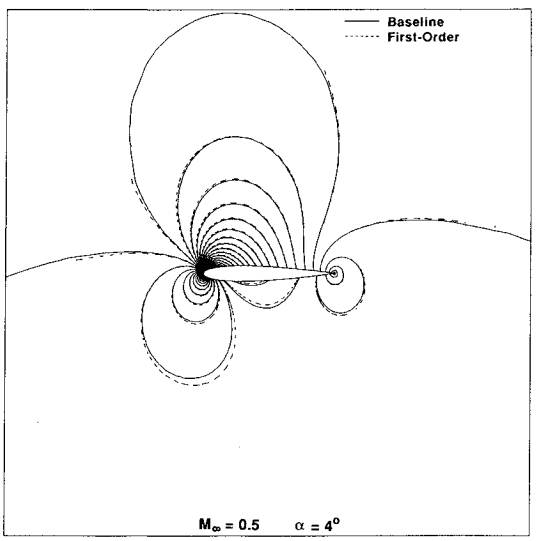

Fig. 5b Pressure contours predicted by ET12D using first-order boundary conditions.

far-field boundary shapes representative of a C-grid topology. Both subsonic and transonic cases have been calculated.

The Euler calculations presented here were carried out for a NACA 0012 airfoil using the ET12D and the FLO672D codes. These two-dimensional codes are derivatives of their three-dimensional counterparts and are based on different numerical solution algorithms.[10,11] The ET12D code uses a Riemann variable formulation and a characteristic-based finite difference solution algorithm. The two-dimensional formulation is given by Eqs. (1–4). The FLO672D code uses a conservative variable formulation and a central difference solution algorithm. Nearly identical results were obtained from these two codes. Implementation in other codes is described in Refs. 8 and 9.

Reference results were calculated using a baseline C grid whose far-field boundaries were located at a large distance (approximately 40 chord lengths) from the airfoil. This distance was sufficiently large so that the zero-order (characteristic) and first-order boundary conditions produced almost identical numerical flowfield predictions. The calculations were repeated on a much smaller core grid using both the zero-order and first-order boundary conditions. The small grid boundaries were very close to the airfoil (approximately one chord). These small grid results are compared with the reference results from the large grid to assess the first-order boundary condition accuracy.

The C portion of the outer boundary for both the reference and core grids was parabolic so that inflow conditions existed at all points along the boundary. The downstream boundary was linear and aligned with the y-coordinate direction as shown in Fig. 1. Outflow conditions existed at all points of this boundary.

The small core grid shown in Fig. 2 had 209 points distributed along the C curves and 41 points in the outward direction. It extended one chord length upstream of the airfoil leading edge and one chord length downstream of the trailing edge. This grid remained unchanged for all of the calculations. The large baseline grid had dimensions 273×65 and was constructed by simply adding parabolic C lines outside of the core grid inflow boundary and vertical lines downstream of the outflow boundary. It extended 40 chord lengths upstream and downstream of the airfoil leading edge. The relative locations of the outer boundaries of the two grids are shown in Fig. 3. The inflow and outflow boundaries could be moved individually or in combination.

Isentropic Flow

Surface Mach numbers predicted by the ET12D and FLO672D codes using the core grid of Fig. 2 are presented in Figs. 4a and 4b. The freestream Mach number for these calculations was 0.50, and the angle of attack was 4 deg. Results for both zero-order and first-order boundary conditions imposed along the boundary $\overline{GHIG}$ (see Fig. 3) are shown. Reference results obtained with the large baseline grid are also included for comparison. The surface pressure comparisons were equally good. Pressure contours predicted by the ET12D code are shown in Figs. 5a and 5b. The first-order conditions used with this extremely small grid produce results that agree well with the reference solution throughout the computational domain. The small grid has 52% fewer grid points than the baseline grid, which reduces computational cost significantly.

Accuracy can be further quantified by comparing computed lift. With the small core grid, the difference in lift from the reference solution was less than 1% for both codes when the first-order boundary conditions were used. Zero-order conditions produced a lift difference of approximately 20%. Figure 6 shows the variation in lift coefficient predicted by the FLO672D code using the zero- and first-order boundary conditions as the downstream boundary location is moved upstream toward the airfoil. With the first-order boundary conditions, the lift coefficient remains essentially constant. With the zero-order boundary conditions, accuracy degrades rapidly as the downstream boundary distance is decreased.

Nonisentropic Flow

With a freestream Mach number of 0.85 and angle of attack of zero, shock waves occur on the upper and lower surfaces of the airfoil. This case was calculated using the ET12D code with the downstream boundary located one chord from the airfoil trailing edge and the overall boundary at $\overline{BCDB}$ (see Fig. 3). Zero-order and first-order nonisentropic boundary conditions were imposed on the downstream boundary $\overline{BD}$. A reference solution was also calculated using the large baseline grid. For this case the vorticity wake produced by the shock waves persists downstream to infinity and cannot be modeled by decaying perturbations as might be obtained from a model based on irrotational potential flow theory. Attempting to model this wake as it crosses the downstream computational boundary by constant boundary conditions (e.g., zero order) is clearly inconsistent.

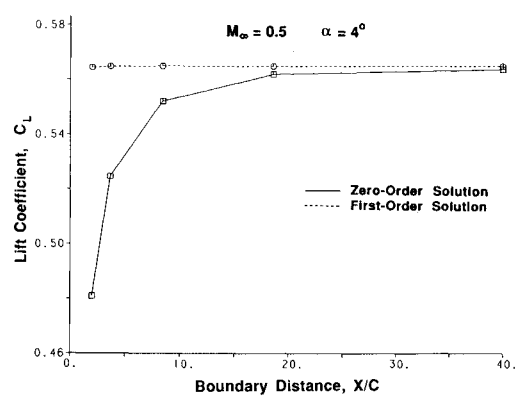

Fig. 6 Effect of downstream boundary location on lift coefficient (FLO672D).

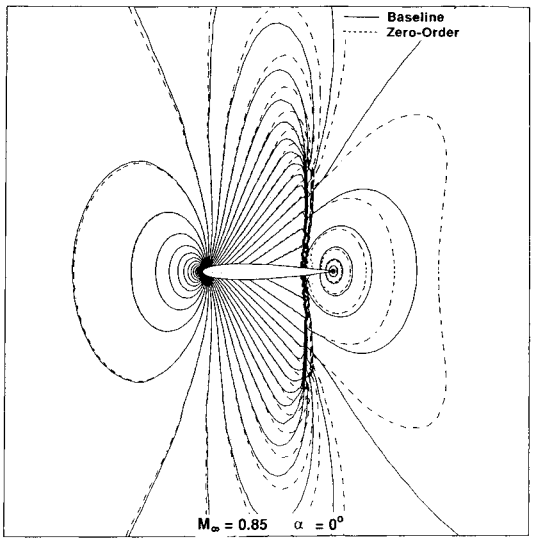

Fig. 7a Pressure contours predicted by ET12D using zero-order boundary conditions.

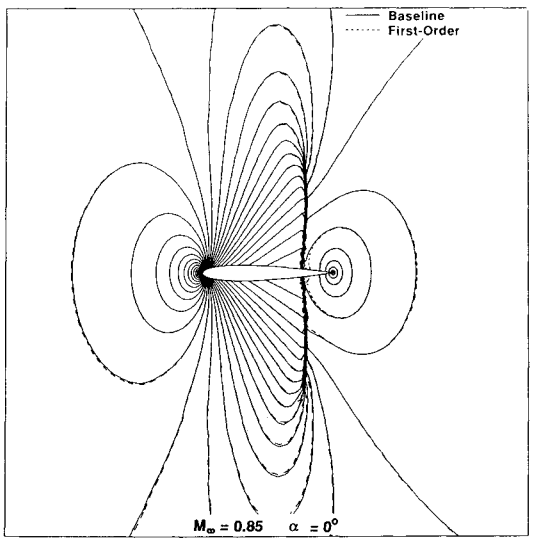

Fig. 7b Pressure contours predicted by ET12D using first-order boundary conditions.

A shock-fitting procedure[12] has been implemented in the ET12D code that produces very accurate transonic flowfield predictions. Since it tracks the shock further into the field than a typical shock-capturing method, the parabolic inflow boundary could not be moved to the $\overline{GHI}$ location. Pressure contours comparing results using zero- and first-order boundary conditions with the reference solution are shown in Figs. 7a and 7b, respectively. Very accurate results are obtained on the small grid when the first-order conditions are used. The most noticeable effect of the zero-order boundary conditions is the incorrect prediction of the shock location and strength. Entropy contours, as shown in Ref. 9, further confirm the accuracy of the boundary condition procedures.

Surface Mach numbers predicted by FLO672D using the small core grid $\overline{GHIG}$ are presented in Fig. 8. The shock waves

are captured with this code, and their interaction with the inflow boundary GHI is not significant. The first-order conditions used with this small grid produce results that agree well with the reference solution. The incorrect shock location caused by the zero-order boundary conditions is apparent.

The linearized thermodynamic relations and iterative solution procedure used in obtaining the boundary conditions (60) do not appear detrimental. The drag computed using the first-order boundary conditions on the core grid differed by less than 1% from that of the reference solution. Figure 9 shows the variation in drag coefficient predicted by the FLO672D code using the zero- and first-order boundary conditions as the downstream boundary location is moved upstream toward the airfoil. With the first-order boundary conditions, the drag coefficient remains essentially constant. With the zero-order boundary conditions, accuracy degrades rapidly as the downstream boundary distance is decreased.

Discussion

Results presented earlier have shown that large efficiency gains can be achieved by incorporating more accurate far-field boundary conditions into numerical flowfield solution methods. The number of computational grid points for a given accuracy level was reduced by approximately one-half by using first-order conditions. The reduction is potentially greater for three-dimensional applications. Only a modest increase in computational effort (approximately 5%) is required for the first-order conditions. An additional efficiency gain may also be provided in that fewer iterations are typically required for solution convergence because of the closer proximity of the far-field boundaries. These gains have not been quantified precisely because no attempt has yet been made to optimize the implementation with any particular numerical solution algorithm.

The first-order boundary condition procedures are general and can be combined with any inviscid numerical solution method, including potential flow methods. Application to viscous calculations has been demonstrated previously.[8] It is advantageous that the far-field boundary shape be simple to

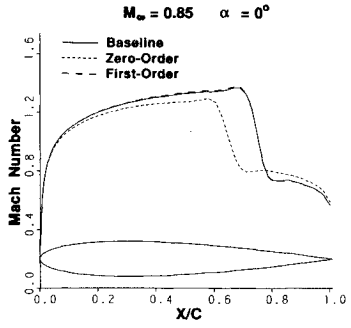

Fig. 8 FLO672D surface Mach number predictions with outer boundary at GHIG.

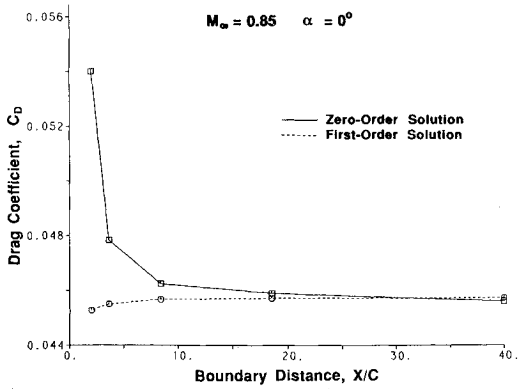

Fig. 9 Effect of downstream boundary location on drag coefficient (FLO672D).

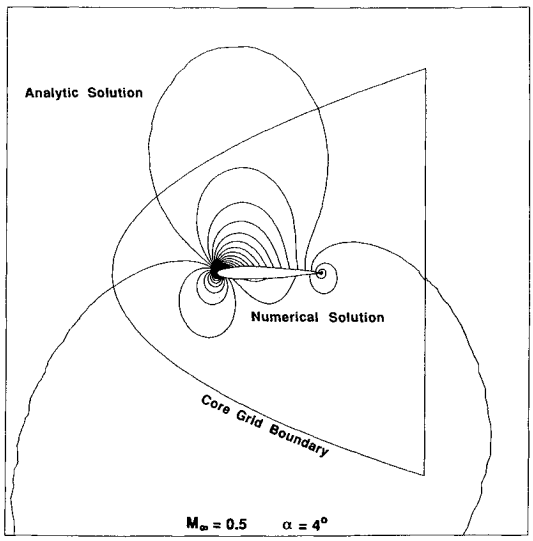

Fig. 10 Pressure contours predicted by ET12D with far-field analytic solution added.

reduce the analytic complexity of the boundary condition procedures. In this respect, the procedures are particularly well suited for unstructured and overlapping grid methods, since outer boundary shapes can be kept relatively simple without placing any burden on the grid generation method.

In deriving the boundary condition procedures, a number of assumptions and simplifying approximations were introduced. Their validity is best judged by the numerical results. For nonisentropic (rotational) flow, the thermodynamic relationships were linearized and an assumption was made that decoupled the energy equation describing entropy convection. The remaining equations were solved approximately by an iterative procedure. Similar approximations were used for internal flow analyses with satisfactory results.[6] A low-order, iterative solution procedure was also used in analyzing the isentropic parabolic boundary as explained earlier. Results presented earlier suggest that these simplifications were not detrimental. Calculated values of lift and drag differed from reference values by less than 1%.

When implementing the first-order boundary conditions, it is necessary to extrapolate into the far field the boundary distributions provided by the nonlinear numerical solution. A simple procedure was suggested earlier. These extrapolated distributions provide only a small contribution to the boundary integrals and any reasonable approximation is sufficient. For a C-grid boundary shape, these extrapolations interact and should be compatible since the far-field solutions overlap. A simplified coupling procedure was used in producing the results presented herein, and no attempt has been made to optimize the coupling. Consistency of the procedure is demonstrated by the pressure contours shown in Fig. 10. Near-field contours of the ET12D computation on the core grid match smoothly with far-field contours of the analytic solutions.

Summary

Far-field computational boundary conditions have been developed for two-dimensional external flow problems. These first-order boundary conditions are derived from analytic solutions of the linearized Euler equations and represent a logical asymptotic extension of the zero-order (or characteristic) boundary conditions commonly used in the numerical solution of nonlinear fluid dynamic equations. The boundary conditions and analytic solutions provide a smooth transition across a computational boundary to the true far-field conditions at infinity. The boundary procedure is general in that it can be used in conjunction with any inviscid numerical solution method. Use of different Euler codes having different numerical solution algorithms have demonstrated this versatility.

The first-order boundary conditions allow the far-field boundaries to be located much closer, thereby reducing the number of grid points needed for the numerical solution and also the number of iterations for solution convergence. This allows a significant reduction in the amount of computational effort required for the nonlinear numerical solution because the additional calculations required for the first-order boundary conditions are modest. Results were shown where the number of grid points was reduced by approximately 50%.

Because the boundary conditions are derived from the Euler equations, the flow crossing the boundaries can be rotational (nonisentropic), and the equations can be used for calculating transonic flows containing shock waves. Several approximations were made in deriving the nonisentropic boundary conditions. The numerical results presented support the validity of these approximations. Representing the vorticity distribution of a viscous wake as an entropy distribution allows the boundary procedures to be used for viscous calculations.

The procedures used for deriving the boundary conditions can be applied to boundary shapes other than the parabolic and linear shapes presented herein. It is advantageous that the far-field boundary shape be simple to reduce the analytic complexity of the boundary condition procedures. In this respect the procedures are particularly well suited for unstructured grid methods since outer boundary shapes can be kept relatively simple without placing any burden on the grid generation method.

References

[1]Engquist, B., and Majda, A., "Absorbing Boundary Conditions for the Numerical Simulation of Waves," *Mathematics of Computation,* Vol. 31, No. 139, 1977, pp. 629–651.

[2]Higdon, R. L., "Initial-Boundary Value Problems for Linear Hyperbolic Systems," *SIAM Review,* Vol. 28, No. 2, 1986, pp. 177–217.

[3]Giles, M. B., "Nonreflecting Boundary Conditions for Euler Equation Calculations," *AIAA Journal,* Vol. 28, No. 12, 1990, pp. 2050–2058.

[4]Hirsch, C., and Verhoff, A., "Far-Field Numerical Boundary Conditions for Internal and Cascade Flow Computations," AIAA Paper 89-1943, June 1989.

[5]Ferm, L., "Open Boundary Conditions for Stationary Inviscid Flow Problems," *Journal of Computational Physics,* Vol. 78, No. 1, 1988, pp. 94–113.

[6]Verhoff, A., and Stookesberry, D., "Far-Field Computational Boundary Conditions for Internal Flow Problems," Naval Postgraduate School, NPS67-88-001CR, Monterey, CA, Sept. 1988.

[7]Verhoff, A., and O'Neil, P. J., "A Natural Formulation for Numerical Solution of the Euler Equations," AIAA Paper 84-0163, Jan. 1984.

[8]Verhoff, A., Stookesberry, D., and Agrawal S., "Far-Field Computational Boundary Conditions for Transonic Flows," 4th International Symposium on Computational Fluid Dynamics, Davis, CA, Sept. 9–12, 1991.

[9]Verhoff, A., Stookesberry, D., and Agrawal S., "Far-Field Computational Boundary Conditions for External Flow Problems," AIAA Paper 91-0630, Jan. 1991.

[10]Agrawal, S., Vermeland, R. E., Verhoff, A., and Lowrie, R. B., "Euler Transonic Solutions over Finite Wings," AIAA Paper 88-0009, Jan. 1988.

[11]Jameson, A., "A Vertex Based Multigrid Algorithm for Three-Dimensional Flow Calculations," *ASME AMD,* Vol. 78, American Society of Mechanical Engineers, New York, Dec. 1986, pp. 45–73.

[12]Moretti, G., "A Technique for Integrating the Two-Dimensional Euler Equations," *Computers and Fluids,* Vol. 15, No. 1, 1987, pp. 59–75.